Hindawi Publishing Corporation
Active and Passive Electronic Components
Volume 2012, Article ID 459043, 10 pages
doi:10.1155/2012/459043

*Research Article*

# GaN-Based High-$k$ Praseodymium Oxide Gate MISFETs with $P_2S_5/(NH_4)_2S_X$ + UV Interface Treatment Technology

**Chao-Wei Lin and Hsien-Chin Chiu**

*Department of Electronics Engineering, Chang Gung University, Taoyuan, Taiwan*

Correspondence should be addressed to Hsien-Chin Chiu, hcchiu@mail.cgu.edu.tw

Received 1 July 2012; Revised 28 September 2012; Accepted 26 October 2012

Academic Editor: Pei-Wen Li

Copyright © 2012 C.-W. Lin and H.-C. Chiu. This is an open access article distributed under the Creative Commons Attribution License, which permits unrestricted use, distribution, and reproduction in any medium, provided the original work is properly cited.

This study examines the praseodymium-oxide- ($Pr_2O_3$-) passivated AlGaN/GaN metal-insulator-semiconductor high electron mobility transistors (MIS-HEMTs) with high dielectric constant in which the AlGaN Schottky layers are treated with $P_2S_5/(NH_4)_2S_X$ + ultraviolet (UV) illumination. An electron-beam evaporated $Pr_2O_3$ insulator is used instead of traditional plasma-assisted chemical vapor deposition (PECVD), in order to prevent plasma-induced damage to the AlGaN. In this work, the HEMTs are pretreated with $P_2S_5/(NH_4)_2S_X$ solution and UV illumination before the gate insulator ($Pr_2O_3$) is deposited. Since stable sulfur that is bound to the Ga species can be obtained easily and surface oxygen atoms are reduced by the $P_2S_5/(NH_4)_2S_X$ pretreatment, the lowest leakage current is observed in MIS-HEMT. Additionally, a low flicker noise and a low surface roughness (0.38 nm) are also obtained using this novel process, which demonstrates its ability to reduce the surface states. Low gate leakage current $Pr_2O_3$ and high-$k$ AlGaN/GaN MIS-HEMTs, with $P_2S_5/(NH_4)_2S_X$ + UV illumination treatment, are suited to low-noise applications, because of the electron-beam-evaporated insulator and the new chemical pretreatment.

## 1. Introduction

Because of their inherent high breakdown voltage ($V_{BR}$), high two-dimensional electron gas (2-DEG) concentration, and high saturation velocity [1, 2], and AlGaN/GaN high electron mobility transistors (HEMTs) are suitable to high-power and low-noise applications. The major factors that limit the performance and reliability of GaN-based HEMTs at radio frequencies (RF) are their high gate leakage current and drain current collapse, which is associated with native oxide-induced surface states [3, 4]. Therefore, AlGaN/GaN metal-insulator-semiconductor HEMTs (MIS-HEMTs), in which $SiO_2$ [5], $Si_3N_4$ [6], $Ga_2O_3$ [7], $Al_2O_3$ [8], and $Sc_2O_3$ [9] are used as the gate dielectrics, are studied, in order to address these problems. Related works focus on the formation of a high-$k$ insulator, which reduces the Schottky gate leakage current at high input signal swings and improves channel modulation. However, the treatment of the interface between AlGaN and the insulator has not been studied systematically. Pretreatment before the deposition of the passivating layer between the source, the drain, and the gate terminals is dominated by the effect of surface traps, which cause flicker noise and current collapse problems. For example, $(NH_4)_2S_X$ sulfide treatment is known to eliminate native $Ga_2O_3$ and $As_2O_3$ dangling bonds on GaAs- and InP-related semiconductors, because of the formation of stable Ga-S and As-S bonds during immersion [10, 11]. In this work, a $P_2S_5/(NH_4)_2S_X$ + UV treatment that suppresses surface traps is studied. Furthermore, to increase the efficiency of the $P_2S_5/(NH_4)_2S_X$ treatment, the treatment is performed in a UV chamber and both the high-$k$ ($\varepsilon \sim 10$) $Pr_2O_3$ gate insulator and the passivating layer are deposited using electron-beam evaporation, which effectively prevents the plasma-induced generation of surface states. A comparison of the flicker noise determined from the pulsed $I$-$V$ of $Pr_2O_3$ AlGaN/GaN MIS-HEMT with that of traditional GaN HEMTs shows that the surface traps are markedly suppressed by $P_2S_5/(NH_4)_2S_X$ + UV treatment. The observed lower surface leakage current also improves the DC-RF dispersion of MIS-HEMT. X-ray photoelectron spectroscopy (XPS) measurement and secondary ion mass spectrometry (SIMS) are used to study the Ga-S energy bonds and the

distributions of the depths of oxygen and sulfur atoms, following $P_2S_5/(NH_4)_2S_X$ + UV treatment.

## 2. Device Structure and Fabrication

The AlGaN/GaN HEMT heterostructures used in this study were grown using atmospheric pressure metal organic chemical vapor deposition (AP-MOCVD) on 2 inch sapphire wafers. The 4000 nm-thick undoped GaN was grown first, to form the buffer and channel layers. Then, a 35 nm-thick undoped $Al_{0.25}Ga_{0.75}N$ layer was grown as the Schottky layer. The designed structure had a sheet charge density of 1.65 $\times$ $10^{13}$ $cm^{-2}$ and a Hall mobility of 1060 $cm^2$/V-s at 300 K. Figure 1 shows the cross-sections of a $Pr_2O_3$/AlGaN/GaN MIS-HEMT with $P_2S_5/(NH_4)_2S_X$ + UV interface pretreatment. During fabrication of the device, the active region was protected by a photoresist and the mesa isolation region was removed using a $BCl_3$ + $Cl_2$ mixture gas plasma in a reactive ion etching (RIE) chamber. The ohmic contacts of the Ti/Al/Ni/Au (25 nm/125 nm/50 nm/100 nm) metal layers were deposited using electron-beam evaporation and patterned by conventional optical lithography and lift-off method, followed by 850°C RTA annealing for 30 s in an $N_2$ environment. Before the deposition of the high-*k* $Pr_2O_3$ insulator and the passivating layers, the samples were immersed in a standard treatment (dilute HCl), $(NH_4)_2S_X$ and $P_2S_5/(NH_4)_2S_X$ for 15 min. Figure 2 shows the pH value of the $P_2S_5/(NH_4)_2S_X$ solution versus $P_2S_5$ weight. The pH of the saturated $(NH_4)_2S_X$ solution is 11.2 and the pH of the mixed $P_2S_5/(NH_4)_2S_X$ solution was adjusted to a value of 7 by adding 10 g of $P_2S_5$ into 30 mL $(NH_4)_2S_X$ saturated solution. Although the $(NH_4)_2S_X$ treatment effectively removes the native AlGaN surface oxide layer, it cannot prevent the increase in surface roughness that is caused by the alkaline $(NH_4)_2S_X$ solution. After 15 min of pretreatment immersion, the AlGaN surface roughness was 0.24 nm for the standard treatment and 0.51 nm and 0.44 nm for the $(NH_4)_2S_X$ and $P_2S_5/(NH_4)_2S_X$ solution. Therefore, the $P_2S_5/(NH_4)_2S_X$ solution was used as the interface pretreatment solution for the MIS-HEMT. In an earlier study by the authors, the reduction of the number of native oxide-induced dangling bonds on the AlGaN surface, which are difficult to remove at room temperature, was achieved by increasing the temperature of the solution temperature to 60°C, but this increase makes the procedure more complicated and time-consuming. In this study, UV illumination is used during $P_2S_5/(NH_4)_2S_X$ pretreatment immersion, in order to rapidly eliminate the dangling bonds and form Ga-S bonds with high-binding energy. After interface treatment, a 10 nm-thick layer of praseodymium was firstly evaporated, using an optimal oxygen flow rate of 15 sccm. During this stage, the chamber pressure was increased to around $10^{-4}$ Torr. When the chamber pressure was reduced to $3 \times 10^{-6}$ Torr, the conventional Ti/Au (30 nm/150 nm) gate metals were deposited. For comparison, a traditional Ni/Au Schottky gate GaN HEMT was also fabricated. Finally, the Ti/Au (30 nm/300 nm) metals were deposited to form the interconnection and probe pads, and a 200 nm-thick $SiO_2$ layer was deposited to passivate the device. The complete process was also used to fabricate a traditional Ni/Au Schottky gate GaN HEMT, for the purpose of comparison.

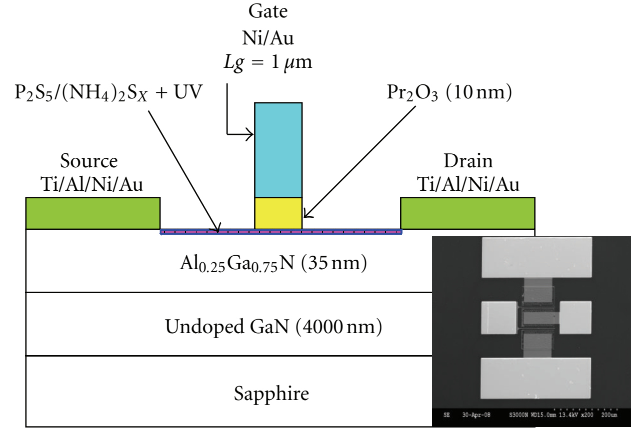


Figure 1: The cross-sectional structure of a $P_2S_5/(NH_4)_2S_X$+UV pretreatment $Pr_2O_3$ MISFET.

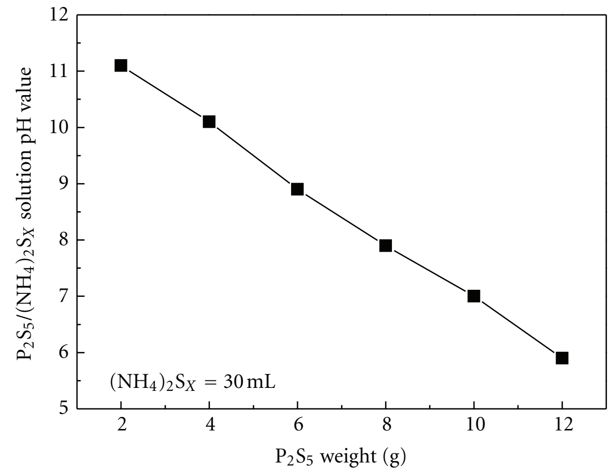


Figure 2: pH value of $P_2S_5/(NH_4)_2S_X$ solution versus $P_2S_5$ weight.

The important optimization of the flow rate of the praseodymium oxide high-*k* layer was also considered. The electron-beam evaporation of the high-*k* $Pr_2O_3$ thin film is optimized by adjusting the oxygen flow rate in the chamber. Figure 3 shows the EDX measurements for $Pr_2O_3$ grown in the electron-beam evaporator using various oxygen flow rates. An analysis of the rare-earth metal atomic concentration in the oxide layer demonstrates that the optimal flow rate for the deposition of the praseodymium oxide layer is 15 standard cubic centimeters per minute (sccm), indicating that the dielectric constant is maximized, because a strong dipole is formed at the highest possible rare-earth metal concentration in the high-*k* oxide layer. The thermal stability of the insulator also plays an important role in high-power GaN MIS-HEMTs because the dc power is primarily dissipated near the gate contact, which causes local Joule self-heating [10]. The channel temperature can reach 100°C during high-output-power operation, which

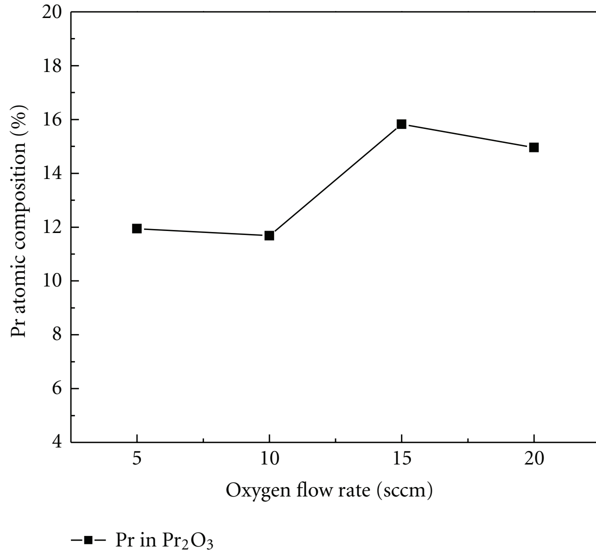


FIGURE 3: EDX analysis of $Pr_2O_3$ films with various oxygen flow rates.

results in increased degradation and failure rates and a reduction in output power. In order to evaluate the thermal stability of $Pr_2O_3$ layer, the X-ray photoelectron spectroscopy (XPS) was used to measure the binding energy of the $Pr_2O_3$ thin films after 400°C, 600°C, and 800°C postannealing. Figure 4(a) shows the XPS 3*d* core-level spectra for $Pr_2O_3$ at various temperatures. The energy of the Ar-gun is 3 KeV, the operation current is 1 mA, and the analysis area is $2 \times 2\ mm^2$. It is seen that the binding energies of the $Pr_2O_3$ after 400°C, 600°C, and 800°C postannealing are close to the standard value of 934 eV in the 3*d* core level, as recorded in the XPS handbook. Figure 4(a) also shows the high signal intensities of $Pr_2O_3$. Therefore, it is concluded that a high-quality and a highly thermally stable high-*k* insulator is obtained by using electron-beam-evaporated Pr with a high oxygen flow rate. The results of high-resolution cross-sectional transmission electron microscopy (TEM) prove that the $Pr_2O_3$ grows on the GaN in a planar fashion, as shown in Figure 4(b). The $Pr_2O_3$ equivalent oxide thickness, measured by the TEM, is 20 nm. A $(Ga_2O_3)Pr_2O_3$ compound film occurs between the interface of the GaN and $Pr_2O_3$ layers, which is generated by the native GaN surface oxide layer and praseodymium materials.

## 3. Experimental Results for the Device

Atomic force microscopy (AFM) or scanning force microscopy (SFM) has a very high resolution, with a demonstrated resolution of the order of fractions of a nanometer, more than 1000 times better than the optical diffraction limit. It is also one of the most widely used tools for imaging, measuring, and manipulating matter at the nanoscale. The information is gathered by "feeling" the surface with a mechanical probe. Piezoelectric elements that facilitate tiny but accurate and precise movements

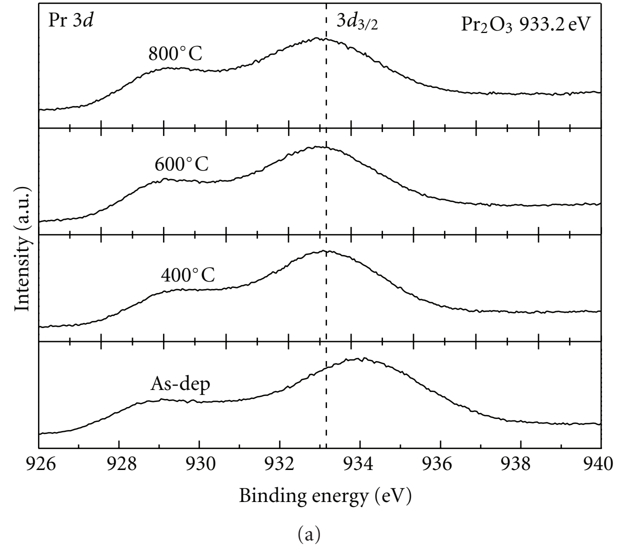


(a)

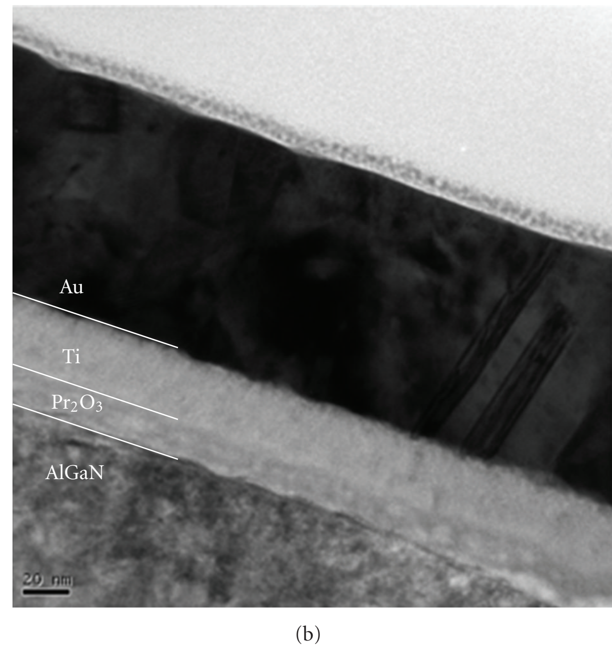


(b)

FIGURE 4: (a) 3*d* core-level XPS spectra of $Pr_2O_3$ versus temperatures. (b) TEM cross-sectional photograph of $Pr_2O_3$ MIS-HEMT.

on (electronic) command enable very precise scanning [11]. Figure 5(a) and Figure 5(b) show the 2D and 3D images of the surface roughness on the AlGaN/GaN surface with different treatments, as measured using a Park Systems XE-70. The $P_2S_5/(NH_4)_2S_X$ + UV-treated surface exhibits a better roughness than the other sulfurization treatments and forms a superior interface between the AlGaN Schottky layer and the $Pr_2O_3$ high-*k* gate insulator layer.

Table 1 shows the mobility, sheet charge density, and surface roughness for variously treated devices, characterized by Hall measurement at 300 K. The $P_2S_5/(NH_4)_2S_X$ + UV-treated devices have a sheet charge density of $1.403 \times 10^{13}\ cm^{-2}$ and a Hall mobility of $1150\ cm^2/V\text{-}s$ at 300 K; these

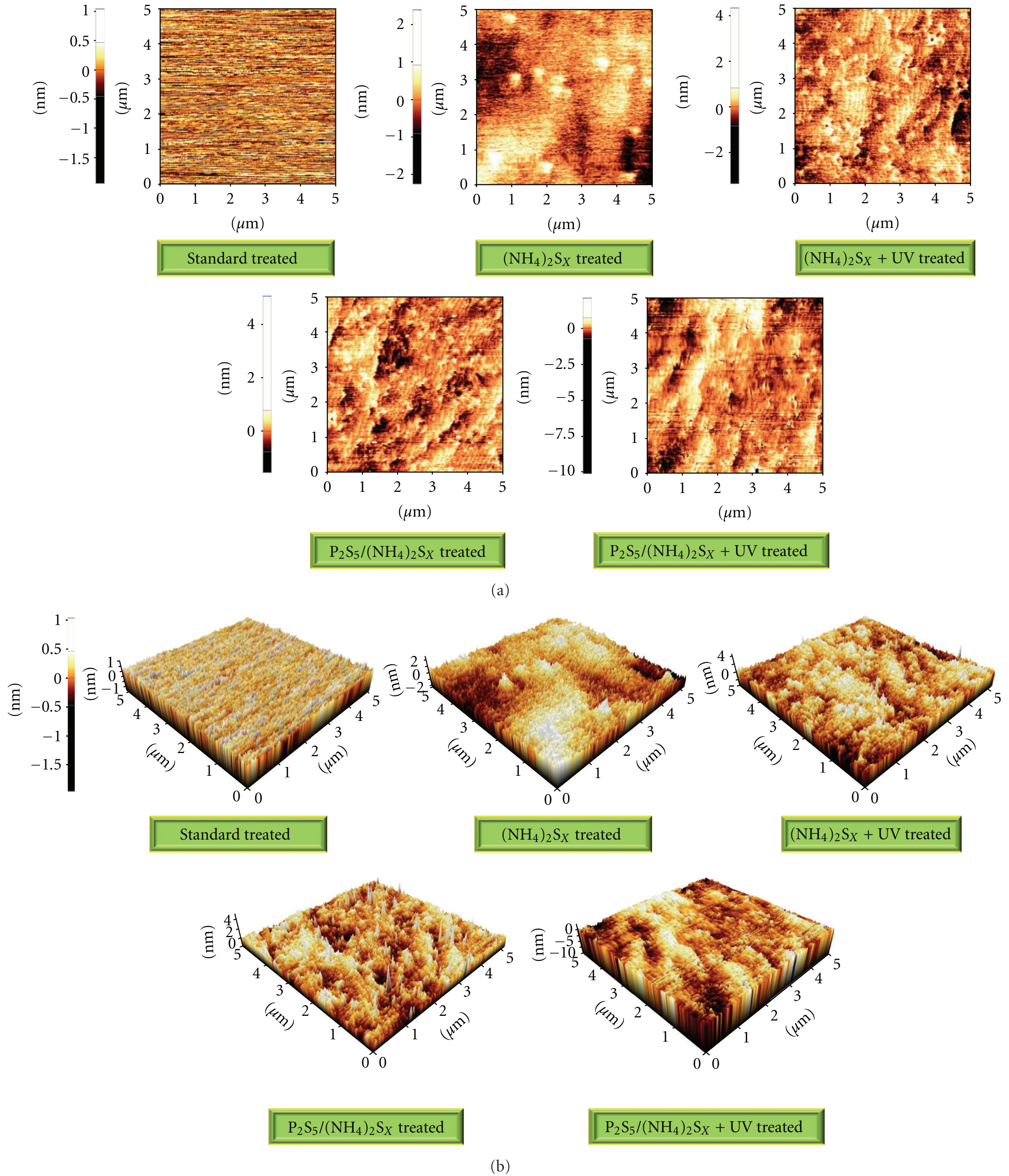


Figure 5: (a) 2D images of the surface roughness on AlGaN/GaN surface evaluated with different treatment. (b) 3D images of the surface roughness on AlGaN/GaN surface evaluated with different treatment.

values are, respectively, $1.648 \times 10^{13}$ cm$^{-2}$, 1060 cm$^2$/V-s and $1.512 \times 10^{13}$, 1087 cm$^2$/V-s for the standard treatment and $(NH_4)_2S_X$ + UV treatment for the devices. These results clearly demonstrate that $P_2S_5/(NH_4)_2S_X$ + UV treatment improves the channel mobility by reducing the number of surface traps.

The surface of composite semiconductor substrates was subject to heat treatment, using an ultraviolet (UV) light,

Table 1: The Hall measurement and surface roughness results for various treatment devices.

| Pretreatment | Mobility ($cm^2$/V-sec) | Sheet charge density ($cm^{-2}$) | Surface roughness (nm) |
|---|---|---|---|
| Standard | 1060 | $1.648 \times 10^{13}$ | 0.238 |
| $(NH_4)_2S_X$ | 985 | $1.784 \times 10^{13}$ | 0.514 |
| $(NH_4)_2S_X$ + UV | 1087 | $1.512 \times 10^{13}$ | 0.471 |
| $P_2S_5/(NH_4)_2S_X$ | 1100 | $1.485 \times 10^{13}$ | 0.443 |
| $P_2S_5/(NH_4)_2S_X$ + UV | 1150 | $1.403 \times 10^{13}$ | 0.382 |

in order to enhance the surface reaction [12]. The photoluminescence (PL) measurements in Figure 6 apply to the complete structure of AlGaN/GaN after sulfurization and demonstrate that $P_2S_5/(NH_4)_2S_X$ + UV treatment yields a greater PL intensity for the AlGaN Schottky layer than either $P_2S_5/(NH_4)_2S_X$ treatment or standard treatment. The increase in PL intensity is due to the elimination of surface states, which generates nonradiative recombination centers on the AlGaN surface [13]. No obvious $Al_{0.25}Ga_{0.75}N$ signal is evident, because the laser used is He-Cd laser and the PL signal intensity of $Al_{0.25}Ga_{0.75}N$ is much smaller than that for GaN. Because only 35 nm AlGaN was grown on GaN for the PL evaluation structure after sulfurization, the $Al_{0.25}Ga_{0.75}N$ signals are not obvious in the PL measurements. Although the $P_2S_5/(NH_4)_2S_X$ treatment can suppress the surface state density, as demonstrated by the PL results, a more concentrated $P_2S_5/(NH_4)_2S_X$ solution with UV illumination treatment produces a stable phosphorus oxide layer and more Ga-S bonds, because the phosphorus and sulfur concentrations are higher [14].

Figure 7 shows the $S_{2p}$ and $Ga_{2p}$ XPS spectra of the variously treated devices. The sulfur $2p$ core level and the binding energy of pure sulfur are all 163.8 eV. The binding energy of gallium is 160 eV at the signal peak in the spectrum of the standard treated GaN sample while the signal peak of the $P_2S_5/(NH_4)_2S_X$-treated device is shifted to 160.3 eV, because the AlGaN surface contains Ga-S bonds (Ga-S = 163.2 eV) after this process. However, $P_2S_5/(NH_4)_2S_X$ + UV treatment shifts the signal peak in the spectrum to 160.4 eV, with a linear distribution of intensity from 160 eV to 161 eV. The $Ga_{2p}$ peaks are shifted to a higher binding energy after $P_2S_5/(NH_4)_2S_X$ + UV treatment. This phenomenon is related to the Ga sulfurized states [15]. Therefore, more Ga-S bonds are generated on the AlGaN surface by $P_2S_5/(NH_4)_2S_X$ + UV treatment than by $P_2S_5/(NH_4)_2S_X$ treatment and these high-energy bonds are more stable than the Ga-O bonds that are formed in a moist environment.

In order to investigate the material atomic composition of the AlGaN surface after various sulfide treatments, the samples were subject to secondary ion mass spectroscopy (SIMS). Figure 8 shows the sulfur and oxygen atom concentration profiles of the samples treated using the three aforementioned methods. Based on the measurement results shown in Figure 8(a), the concentration of S atoms in the $P_2S_5/(NH_4)_2S_X$ and $P_2S_5/(NH_4)_2S_X$ + UV-treated samples

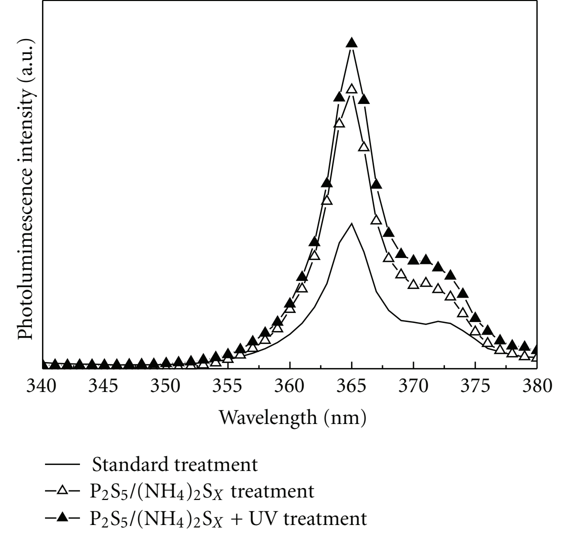


Figure 6: PL measurement results for AlGaN/GaN full structure standard, $P_2S_5/(NH_4)_2S_X$ and $P_2S_5/(NH_4)_2S_X$ + UV treatments.

is relatively high near the AlGaN surface, dropping by two to three orders of magnitude in the channel. However, few S atoms are observed after the standard treatment. The S atoms produced from the sulfide solution are incorporated into the sample surface, which is similar to the effect of the immersion of $CF_4$ in plasma, used to enable a GaN HEMT to operate in enhancement mode [16]. In order to further investigate the mechanism for the removal of Ga-O bonds by sulfur treatments, an experiment was conducted to determine the oxygen concentration distribution; Figure 8(b) shows the results. The lowest curve in the figure shows that the $P_2S_5/(NH_4)_2S_X$ + UV treatment removes a huge amount of AlGaN/GaN native oxide and reduces the number of oxygen atoms more effectively than the other treatments, because UV illumination provides enough energy to the sulfur atoms to replace the Ga-O bonds and form stable Ga-S bonds. Therefore, $P_2S_5/(NH_4)_2S_X$ + UV treatment not only produces a smoother Schottky interface, reducing the gate leakage current, but also reduces the number of oxygen atoms more effectively. Both effects reduce the density of the surface states.

Figure 9 plots the gate-to-drain $I$-$V$ curves for a standard GaN HEMT, a $Pr_2O_3$ MIS-HEMT, and a $P_2S_5/(NH_4)_2S_X$ + UV-treated $Pr_2O_3$ MIS-HEMT. A reduction in the number surface states and leakage current in the sulfide-treated sample means that $P_2S_5/(NH_4)_2S_X$ + UV-treated MIS-HEMTs have a higher $V_{ON}$ value than the others. The improved $V_{ON}$ value of 1.71 V for the $P_2S_5/(NH_4)_2S_X$ + UV-treated $Pr_2O_3$-gate device results in a significant reduction in the gate leakage current at a high pumped gate voltage, which improves the linearity and results in a reduction in the signal dispersion of the device. The reversed gate-to-drain breakdown voltages ($V_{BR}$), defined as the voltage at which the gate leakage current is −1 mA/mm, are −131.3 V for the $P_2S_5/(NH_4)_2S_X$ + UV-treated samples, which allows operation at high drain voltage, and only −128.2 V and

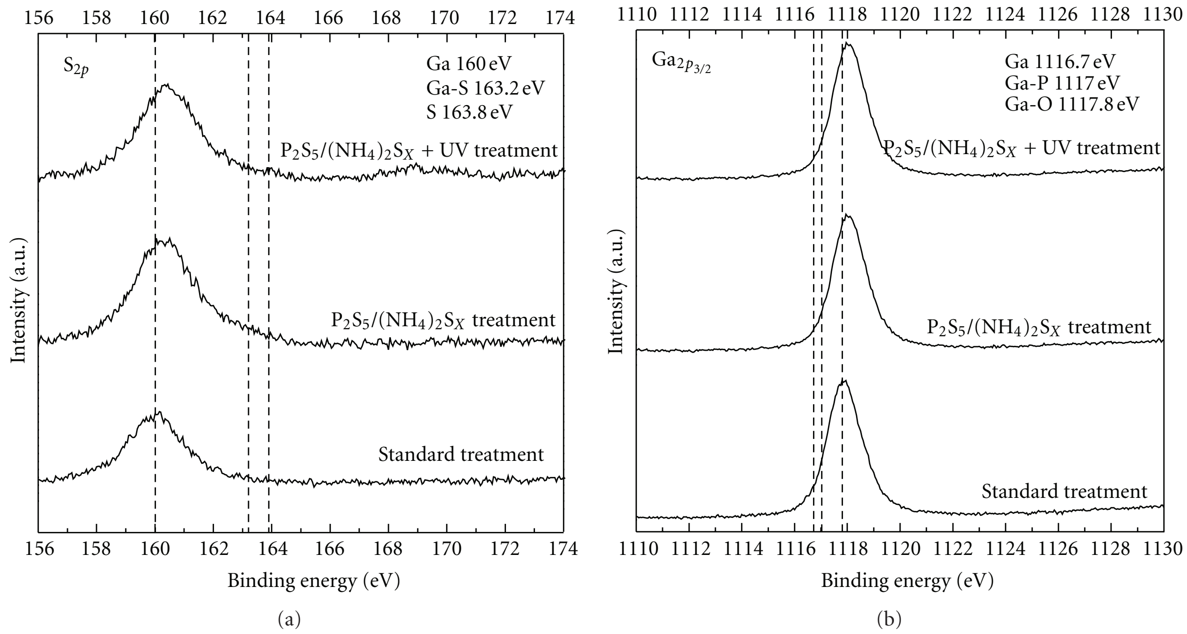


Figure 7: The XPS spectra of $S_{2p}$ (a) and $Ga_{2p}$ (b) and core level of various treatment samples.

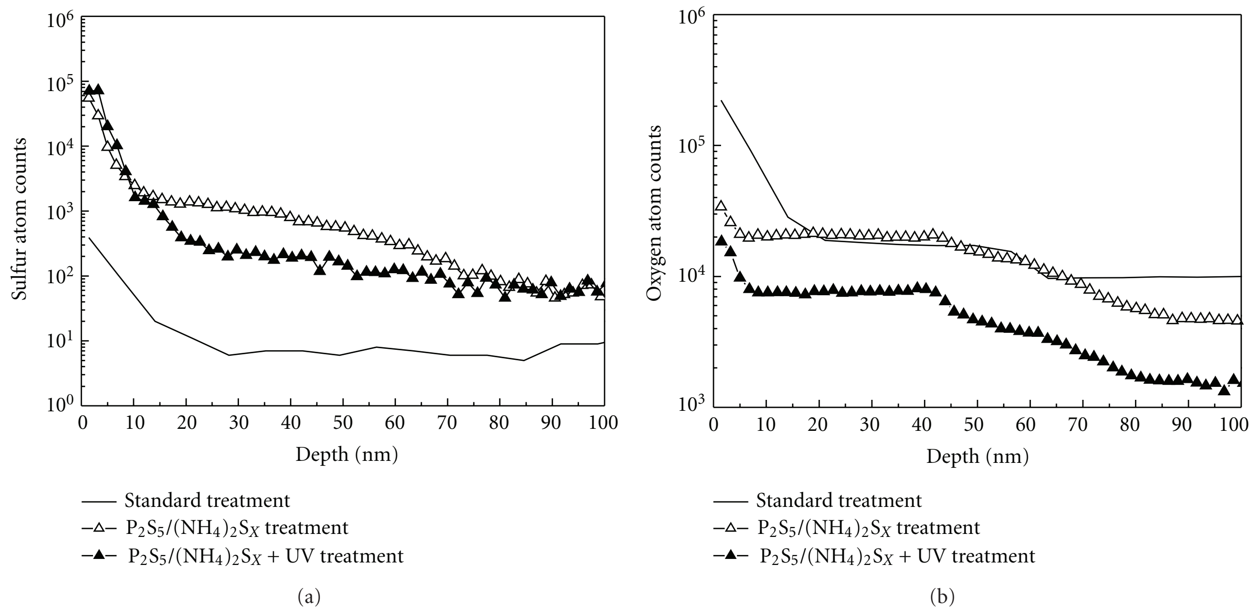


Figure 8: The SIMS measurements of the S atoms (a) and O atoms (b) distribution versus AlGaN/GaN depth for various treatment samples.

−107.5 V for the $Pr_2O_3$ MIS-HEMT and standard-treated samples, respectively.

In order to study the dc characteristics, the drain-to-source current ($I_{ds}$) versus drain-to-source voltage ($V_{ds}$) curves for three devices are shown in Figure 10. The drain current does not vary significantly between the treated devices. The turn-on resistance ($R_{ON}$) is 3.958 Ω for the HEMTs subject to standard treatment, at $V_{gs}$ of 0 V, and 4.675 Ω and 4.210 Ω for the $Pr_2O_3$ MIS-HEMTs and the $P_2S_5/(NH_4)_2S_X$ + UV-treated $Pr_2O_3$ MIS-HEMTs, respectively. This is primarily because the sulfide solution influences only the surface states, rather than the intrinsic parameters. However, since the traps within the interface between the gate and channel are suppressed by $P_2S_5/(NH_4)_2S_X$ + UV treatment, the sample with this treatment has the highest output resistance, which results in an increase in device linearity and power gain cut-off frequency ($f_{max}$). The output conductance ($g_0$) of the $P_2S_5/(NH_4)_2S_X$ + UV-treated

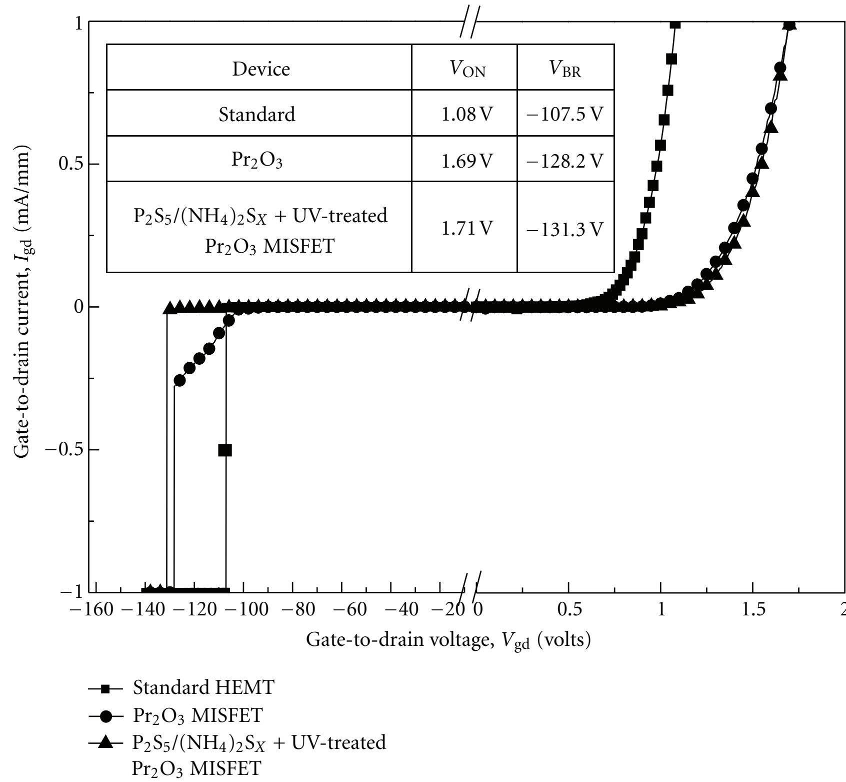


Figure 9: The device gate-to-drain $I$-$V$ characteristics of standard HEMT, $Pr_2O_3$ MISFET, and $P_2S_5/(NH_4)_2S_X$ + UV-treated $Pr_2O_3$ MISFET.

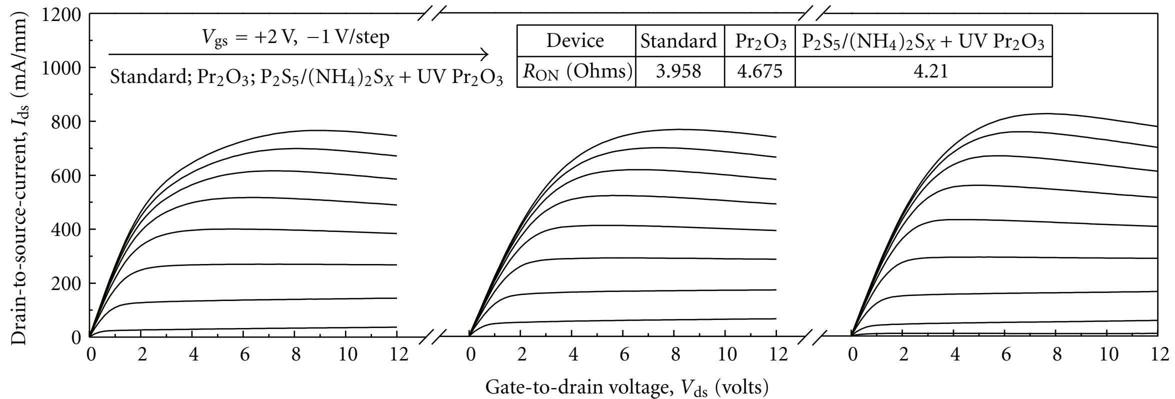


Figure 10: The $I_{ds}$-$V_{ds}$ characteristics of various devices.

$Pr_2O_3$ MIS-HEMTs is 0.46 mS/mm; the corresponding values for the $Pr_2O_3$ MIS-HEMTs and the standard device are 0.6 mS/mm and 1 mS/mm, respectively.

Figure 11 plots the transistor transconductance ($g_m$) versus $V_{gs}$ curves for the three devices of interest at a $V_{ds}$ of 8 V. The maximum drain-to-source currents ($I_{d\,max}$) at $V_{gs} = 4$ V are 923 mA/mm, 864 mA/mm, and 920 mA/mm, for the standard HEMTs, the $Pr_2O_3$ MIS-HEMTs, and the $P_2S_5/(NH_4)_2S_X$ + UV-treated $Pr_2O_3$ MIS-HEMTs, respectively. The maximum transconductance values ($g_m$), biased at $V_{ds} = 8$ V, are 144 mS/mm, 121 mS/mm, and 132 mS/mm, respectively. All of these values are reasonably favorable. The standard HEMTs exhibit a higher peak $g_m$, because a high-$k$ insulator is inserted in the MIS-HEMTs structure. The gate-to-channel improves channel modulation and effectively modulates any increase in the depletion region between the metal gate and the channel. Obviously, high-$k$ GaN MIS-HEMTs demonstrate large swing voltage and low gate leakage current.

The measurement of on-wafer microwave S-parameters for $1 \times 200\,\mu m^2$ devices was performed in a common-source configuration using an Agilent E8364C PNA network analyzer, from 0.1 GHz to 20.1 GHz. S-parameter measurements demonstrate a maximum current gain cut-off frequency ($f_T$) of 9.2 GHz and a maximum oscillation frequency ($f_{max}$) of 16.8 GHz for standard HEMTs. These values are 7.9 GHz

Table 2: The dc and RF characteristics comparisons of a standard HEMT, a $Pr_2O_3$ MISFET, and a $P_2S_5/(NH_4)_2S_X$ + UV-treated $Pr_2O_3$ MISFET.

| Measurement results | Standard | $Pr_2O_3$ | $P_2S_5/(NH_4)_2S_X$ + UV $Pr_2O_3$ |
|---|---|---|---|
| Schottky turn-on voltage ($V_{ON}$) | 1.08 V | 1.69 V | 1.71 V |
| Breakdown voltage ($V_{BR}$) | −107.5 V | −128.2 V | −131.3 V |
| Pinch-off voltage ($V_p$) | −5.8 V | −6.4 V | −6.8 V |
| Maximum drain current ($I_{d\,max}$) | 923.4 mA/mm | 864.4 mA/mm | 920.04 mA/mm |
| Peak transconductance ($g_m$) | 143.58 mS/mm | 121 mS/mm | 132.36 mS/mm |
| Current gain cut-off frequency ($f_T$) | 9.2 GHz | 7.9 GHz | 8.5 GHz |
| Maximum oscillation frequency ($f_{max}$) | 16.8 GHz | 19.2 GHz | 16.2 GHz |

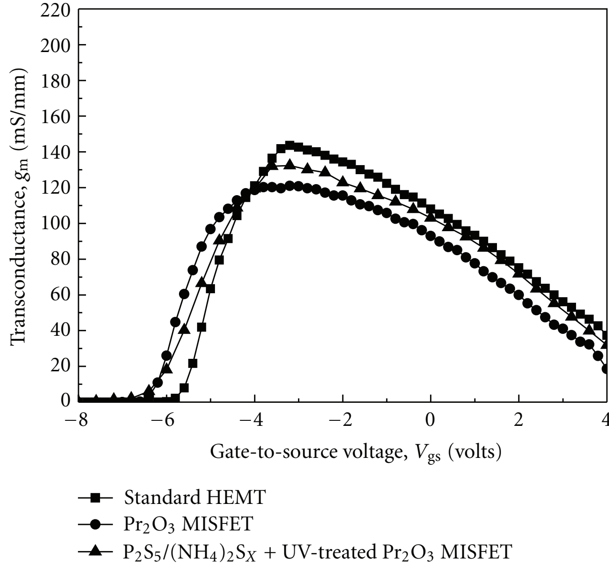


Figure 11: The $g_m$-$V_{gs}$ characteristics of various devices.

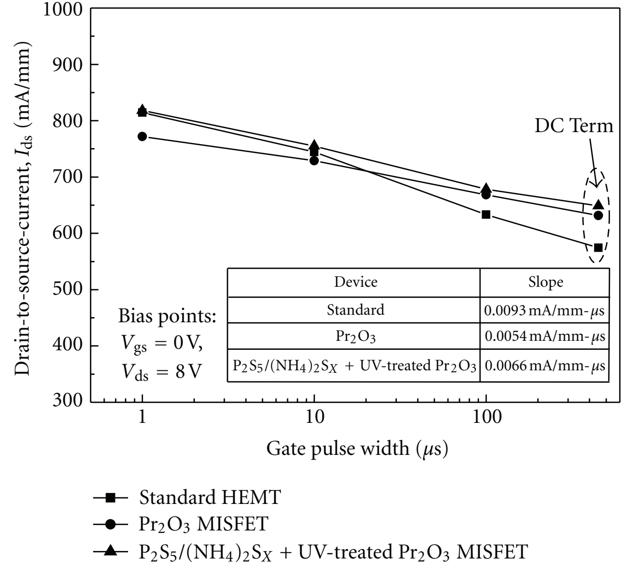


Figure 12: Pulse measurement characteristics of various devices.

and 10.7 GHz for $Pr_2O_3$ MIS-HEMTs and 8.5 GHz and 16.2 GHz for $P_2S_5/(NH_4)_2S_X$ + UV-treated $Pr_2O_3$ MIS-HEMTs, at $V_{ds}$ = 8 V and $V_{gs}$ = −3.2 V, respectively. The superior RF characteristics for $P_2S_5/(NH_4)_2S_X$ + UV-treated $Pr_2O_3$ MIS-HEMTs prove their greater power and linearity. Table 2 presents dc and radio RF characteristics for various devices.

Pulse measurements were made to characterize the carrier trapping phenomenon and heating effect in the device. With respect to the trapping carriers, the response time dominates the pulse measurement. The response time for these trapping carriers is typically of the order of $\mu$s longer than the ns of carrier transportation, especially for high-speed and high-power devices. In order to more easily observe the output signals from the drains of each device, a 50 Ω resistor was added between the drain electrode and the power supply, in order to determine the total drain-to-source current and to reduce the damping effect in the output square waveform. Pulse *I-V* measurements for the three devices were also made, in order to confirm their surface trapping effects. Figure 12 plots the dc to 1 $\mu$s pulse *I-V* measurement for $1 \times 100\,\mu m^2$ devices at a $V_{gs}$ of 0 V and a $V_{ds}$ of 8 V, for the three devices. The gate width of the measured devices is 100 $\mu$m, so the heating effect could therefore be neglected. Since the surface states determine the dispersion effect, the current density at high current decays as the pulse width decreases. As shown in the figure, the standard GaN HEMTs demonstrate a larger slope with respect to the pulse period than do the $Pr_2O_3$ MIS-HEMTs and $P_2S_5/(NH_4)_2S_X$ + UV-treated $Pr_2O_3$ MIS-HEMTs. It is evident that $P_2S_5/(NH_4)_2S_X$ + UV treatment produces reliable and stable surface performance and less load-line hysteresis and better linearity for the device in high-power applications are which both expected.

To investigate the relationship between the flicker noise and the quantity of the variously treated devices, a low-frequency noise measurement was performed, because, at low frequency, this is sensitive to the semiconductor surface [17]. The bias point for low-frequency noise measurement was selected as $V_{ds}$ = 8 V, which gives an $I_{ds}$ of 100 mA/mm for all devices. Since the measurement is dominated by the series resistance of each device, identical $I_{ds}$ bias point confirms the flicker noise characteristics. As shown in Figure 13, the $P_2S_5/(NH_4)_2S_X$ + UV-treated MIS-HEMT demonstrates a lower 1/f spectral noise than both the $Pr_2O_3$ MIS-HEMT and the GaN HEMT, which proves

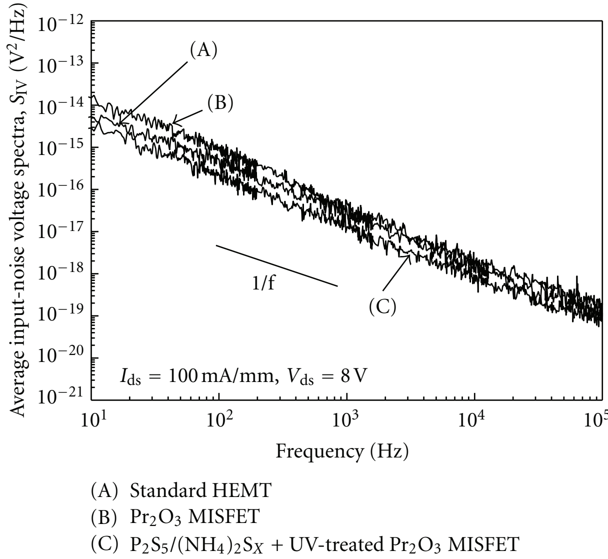


(A) Standard HEMT
(B) $Pr_2O_3$ MISFET
(C) $P_2S_5/(NH_4)_2S_X$ + UV-treated $Pr_2O_3$ MISFET

Figure 13: The 1/f noise comparisons for various devices.

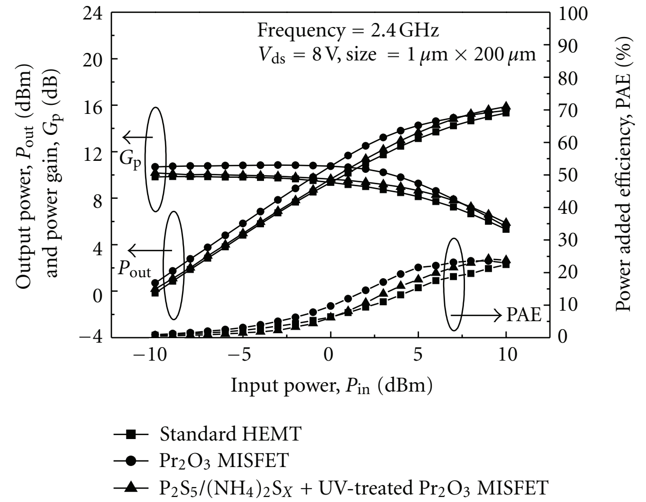


Figure 14: Power performances of three devices under 2.4 GHz and $V_{ds}$ of 8 V operation.

the reduction in the number of surface dangling bonds due to $P_2S_5/(NH_4)_2S_X$ + UV treatment.

The fabricated 1 μm long gate GaN HEMT, $Pr_2O_3$ MIS-HEMT, and $P_2S_5/(NH_4)_2S_X$ + UV-treated $Pr_2O_3$MIS-HEMT were tested on-wafer and the microwave power characteristics were evaluated using a load-pull system with automatic tuners, which simultaneously provides conjugate-matched input and load impedances for the maximum output power. The microwave load-pull power performance was conducted at 2.4 GHz, with a drain bias of 8 V, using various devices. The bias points for class AB operation of the standard HEMT, the $Pr_2O_3$ MIS-HEMT, and the $P_2S_5/(NH_4)_2S_X$ + UV-treated $Pr_2O_3$ MIS-HEMT must be biased at −3.1 V, −3.7 V, and −3.4 V (at 1/4 $I_{d\,max}$), respectively. Figure 14 shows the output power ($P_{out}$), power gain ($G_p$), and PAE as a function of the input power ($P_{in}$), for various devices with gate dimensions of 1 × 200 $\mu m^2$. The $P_2S_5/(NH_4)_2S_X$ + UV-treated $Pr_2O_3$ MIS-HEMT has better dc current and lower gate leakage current than that of the standard HEMT or the $Pr_2O_3$ MIS-HEMT, at high-input-power swing. The PAE values are 22.4%, 23.6%, and 24.2%, for the standard HEMT, the $Pr_2O_3$ MIS-HEMT and the $P_2S_5/(NH_4)_2S_X$ + UV-treated $Pr_2O_3$ MIS-HEMT, respectively. As a result, the microwave-power performance is improved by the MIS-gate structure, and the power-gain degradation is also improved in the high-input-power regime. The reduction in gate leakage current in the $P_2S_5/(NH_4)_2S_X$ + UV-treated $Pr_2O_3$ MIS-HEMT allows a significant improvement in device linearity [18].

## 4. Conclusion

In summary, $Pr_2O_3$ MIS-HEMTs with low gate leakage current and low flicker noise, as a result of $P_2S_5/(NH_4)_2S_X$ + UV treatment, were developed and characterized. An electron-beam-evaporated high-*k* insulator and a passivating layer prevent the formation of surface states by plasma. $P_2S_5/(NH_4)_2S_X$ + UV treatment represents a simple and efficient means of reducing the number of surface dangling bonds. Based on the results of Hall, XPS, and SIMS measurements, this $P_2S_5/(NH_4)_2S_X$ + UV treatment prevents the formation of strong Ga-S bonds on the AlGaN surface. This reduction in surface states improves carrier mobility and simultaneously suppresses unstable native Ga-O bonds. This novel pretreatment is therefore proven to be eminently suitable to low-noise GaN MIS-HEMT applications.

## Acknowledgments

The authors would like to thank the Nano Device Labs (NDL) for providing the low frequency noise measurements, and the National Central University (NCU) for providing the thermal image measurements. This work was financially supported by the National Science Council, ROC [NSC-97-2221-E-182-048-MY3 and NSC-100-2221-E-182-009], and High Speed Intelligent Communication (HSIC) Research Center of Chang Gung University, Taoyuan, Taiwan.

## References

[1] T. P. Chow and R. Tyagi, "Wide bandgap compound semiconductors for superior high-voltage unipolar power devices," *IEEE Transactions on Electron Devices*, vol. 41, no. 8, pp. 1481–1483, 1994.

[2] S. J. Pearton, J. C. Zolper, R. J. Shul, and F. Ren, "GaN: processing, defects, and devices," *Journal of Applied Physics*, vol. 86, no. 1, pp. 1–78, 1999.

[3] M. F. Romero, A. Jiménez, J. Miguel-Sánchez et al., "Effects of $N_2$ plasma pretreatment on the SiN passivation of AlGaN/GaN HEMT," *IEEE Electron Device Letters*, vol. 29, no. 3, pp. 209–211, 2008.

[4] C. Rongming, S. Likun, N. Fichtenbaum et al., "Correlation between DC-RF dispersion and gate leakage in deeply recessed GaN/AlGaN/GaN HEMTs," *IEEE Electron Device Letters*, vol. 29, no. 4, pp. 303–305, 2008.

[5] M. A. Khan, X. Hu, A. Tarakji, G. Simin, and J. Yang, "AlGaN/GaN metal-oxide-semiconductor heterostructure field-effect transistors on SiC substrates," *Applied Physics Letters*, vol. 77, no. 9, pp. 1339–1341, 2000.

[6] X. Hu, A. Koudymov, G. Simin et al., "$Si_3N_4$/AlGaN/GaN-metal-insulator-semiconductor heterostructure field-effect transistors," *Applied Physics Letters*, vol. 79, no. 17, pp. 2832–2834, 2001.

[7] C. T. Lee, H. W. Chen, and H. Y. Lee, "Metal-oxide-semiconductor devices using $Ga_2O_3$ dielectrics on *n*-type GaN," *Applied Physics Letters*, vol. 82, no. 24, pp. 4304–4306, 2003.

[8] P. D. Ye, B. Yang, K. K. Ng et al., "GaN metal-oxide-semiconductor high-electron-mobility-transistor with atomic layer deposited $Al_2O_3$ as gate dielectric," *Applied Physics Letters*, vol. 86, no. 6, Article ID 063501, pp. 1–3, 2005.

[9] R. Mehandru, B. Luo, J. Kim et al., "AlGaN/GaN metal-oxide-semiconductor high electron mobility transistors using $Sc_2O_3$ as the gate oxide and surface passivation," *Applied Physics Letters*, vol. 82, no. 15, pp. 2530–2532, 2003.

[10] H. C. Chiu, C. S. Cheng, and Y. J. Shih, "High uniformity $(Al_{0.3}Ga_{0.7})_{0.5}In_{0.5}P$/InGaAs enhancement-mode pseudomorphic HEMTs by selective succinic acid gate recess," *Electrochemical and Solid-State Letters*, vol. 9, no. 2, pp. G59–G61, 2006.

[11] L. B. Chang, C. H. Chang, M. J. Jeng, H. C. Chiu, and H. F. Kuo, "Barrier height enhancement of $Al_xGa_{1-x}N$/GaN schottky diodes prepared by $P_2S_5(NH_4)_2S$ treatments," *Electrochemical and Solid-State Letters*, vol. 10, no. 3, pp. H79–H81, 2007.

[12] M. J. Jeng, H. T. Wang, L. B. Chang, and R. M. Lin, "Surface passivation using $P_2S_5/(NH_4)_2S_x$ and hydrogen fluoride solutions on Ag/n-InAs and Ag/n-InSb Schottky diodes," *Japanese Journal of Applied Physics*, vol. 40, no. 2, pp. 562–564, 2001.

[13] S. L. Chang and J. F. Kauffman, "Excitation power dependence of photoluminescence enhancement from passivated GaAs," *Applied Physics Letters*, vol. 66, no. 25, pp. 3504–3506, 1995.

[14] H. C. Chiu, Y. C. Huang, C. W. Chen, and L. B. Chang, "Electrical characteristics of passivated Pseudomorphic HEMTs with $P_2S_5/(NH_4)_2S_x$ pretreatment," *IEEE Transactions on Electron Devices*, vol. 55, no. 3, pp. 721–726, 2008.

[15] X. Y. Hou, W. Z. Cai, Z. Q. He et al., "Electrochemical sulfur passivation of GaAs," *Applied Physics Letters*, vol. 60, no. 18, pp. 2252–2254, 1992.

[16] Y. Cai, Y. Zhou, K. J. Chen, and K. M. Lau, "High-performance enhancement-mode AlGaN/GaN HEMTs using fluoride-based plasma treatment," *IEEE Electron Device Letters*, vol. 26, no. 7, pp. 435–437, 2005.

[17] Y. J. Chan and D. Pavlidis, "Trap studies in GaInP/GaAs and AlGaAs/GaAs HEMT's by means of low-frequency noise and transconductance dispersion characterizations," *IEEE Transactions on Electron Devices*, vol. 41, no. 5, pp. 637–642, 1994.

[18] C. W. Lin, H. C. Chiu, C. K. Lin, and J. S. Fu, "High-k praseodymium oxide passivated AlGaN/GaN MOSFETs using $P_2S_5/(NH_4)_2S_x$ + UV interface treatment," *Microelectronics Reliability*, vol. 51, no. 2, pp. 381–385, 2011.

Journal of
Engineering

The Scientific
World Journal
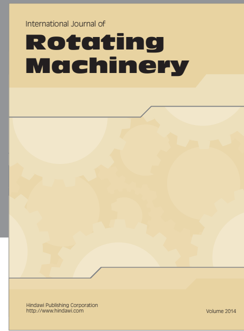
International Journal of
Rotating
Machinery

Journal of
Sensors

International Journal of
Distributed
Sensor Networks
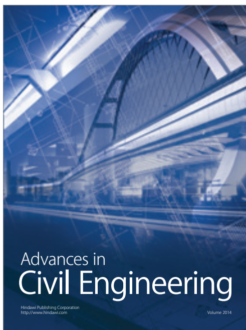
Advances in
Civil Engineering

Hindawi
Submit your manuscripts at
http://www.hindawi.com
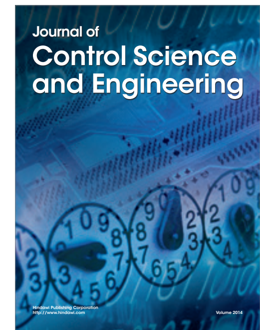
Journal of
Control Science
and Engineering

Journal of
Robotics
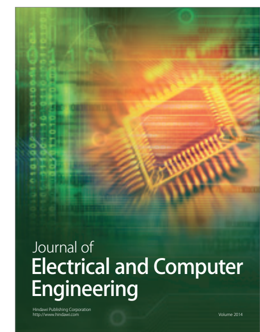
Journal of
Electrical and Computer
Engineering
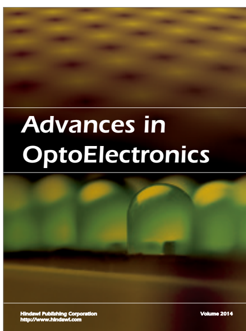
Advances in
OptoElectronics

VLSI Design

International Journal of
Navigation and
Observation
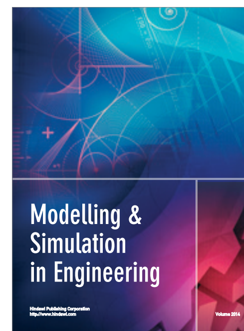
Modelling &
Simulation
in Engineering

International Journal of
Aerospace
Engineering

International Journal of
Chemical Engineering
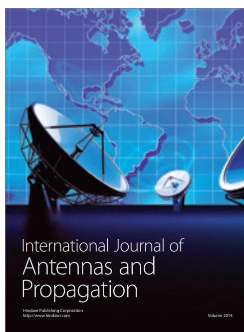
International Journal of
Antennas and
Propagation
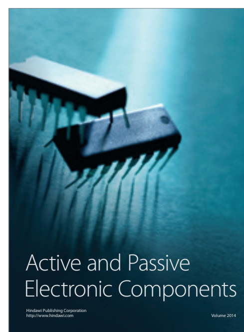
Active and Passive
Electronic Components
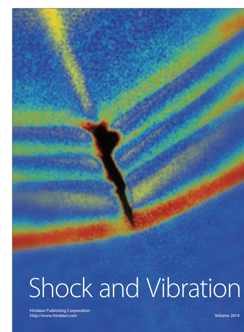
Shock and Vibration
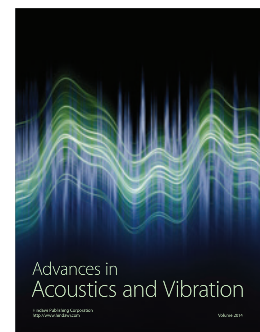
Advances in
Acoustics and Vibration